

Refining Generative Process with Discriminator Guidance in Score-based Diffusion Models

Dongjun Kim^{*1} Yeongmin Kim^{*1} Wanmo Kang¹ Il-Chul Moon¹

Abstract

While the success of diffusion models has been witnessed in various domains, only a few works have investigated the variation of the generative process. In this paper, we introduce a new generative process that is closer to the reverse process than the original generative process, given the identical score checkpoint. Specifically, we adjust the generative process with the auxiliary discriminator between the real data and the generated data. Consequently, the adjusted generative process with the discriminator generates more realistic samples than the original process. In experiments, we achieve new SOTA FIDs of 1.74 on CIFAR-10, 1.33 on CelebA, and 1.88 on FFHQ in the unconditional generation.

1. Introduction

The diffusion model has recently been highlighted for its success in image generation (Dhariwal & Nichol, 2021; Ho et al., 2021; Karras et al., 2022; Song et al., 2020), video generation (Singer et al., 2022; Ho et al., 2022; Voleti et al., 2022), and text-to-image generation (Rombach et al., 2022; Ramesh et al., 2022; Saharia et al., 2022). The State-Of-The-Art (SOTA) models perform human-level generation, but there is still much room to investigate further for a deep understanding of diffusion models.

Contrastive to previous frameworks such as VAEs (Kingma & Welling, 2013) and GANs (Goodfellow et al., 2020), diffusion models generate a sample by solving the generative process in Figure 1-(a), which is a trained Stochastic Differential Equation (SDE). The SDE solver needs numerous evaluations of the score network, so reducing the required number of evaluations is one of the critical problems in diffusion models. For an orthogonal research direction in sampling, enhancing the sample quality given the same sampling budget could be an attractive topic in diffusion models.

^{*}Equal contribution ¹Department of Industrial and Systems Engineering, KAIST, Daejeon, South Korea. Correspondence to: Dongjun Kim <dongjoun57@kaist.ac.kr>.

This paper focuses on the latter topic to improve the generation. We introduce an adjusted generative process in Figure 1-(b) (Eq. (7)), and we approximate this process with a discriminator as in Eq. (11). In detail, we add the gradient of the log density ratio $\nabla \log \frac{p_r^t}{p_g^t} \approx \nabla \log \frac{d_\phi}{1-d_\phi}$ (d_ϕ : discriminator) to the score network s_θ in our generative process, where p_r^t and p_g^t are the probability distributions of the data and sample variables, respectively. In the generation process, the density ratio is maximized from the adjustment. Therefore, given that the samples of higher density ratio $\frac{p_r^t}{p_g^t}$ are visually more realistic than those of lower density ratio in Figure 2, the adjusted process leads more realistic samples. Theoretically, this adjustment certainly alleviates the score estimation error in Theorem 2. Moreover, under a mild condition, the proposed process matches to the exact reverse process in Theorem 1. In experiments, we achieve SOTA FIDs on CIFAR-10 (Krizhevsky et al., 2009), CelebA (Liu et al., 2015), and FFHQ (Karras et al., 2019) for unconditional image generation.

2. Preliminary and Related Works

The forward diffusion process perturbs the data variable into a noise variable by adding an iterative Gaussian noise (Ho et al., 2020; Dhariwal & Nichol, 2021), i.e.,

$$\mathbf{x}_{t+1} = \sqrt{1 - \beta_t} \mathbf{x}_t + \beta_t \epsilon, \quad (1)$$

where ϵ follows a standard Gaussian distribution $\mathcal{N}(0, \mathbf{I})$, t is integer index for intermediate perturbed variables, and β_t determines the perturbing speed. In the continuous limit (Song et al., 2020), this diffusion process can be formulated as a stochastic differential equation of

$$d\mathbf{x}_t = -\frac{1}{2}\beta_t \mathbf{x}_t dt + g_t d\mathbf{w}_t, \quad (2)$$

with t being a continuum of the diffusion index in $[0, T]$, and g_t to be a volatility coefficient. With this continuous perspective, the discrete diffusion process in Eq. (1) (Ho et al., 2020) becomes a discretized process of Eq. (2). In this paper, we describe our model with a continuous viewpoint mainly for the notational simplicity. We emphasize that

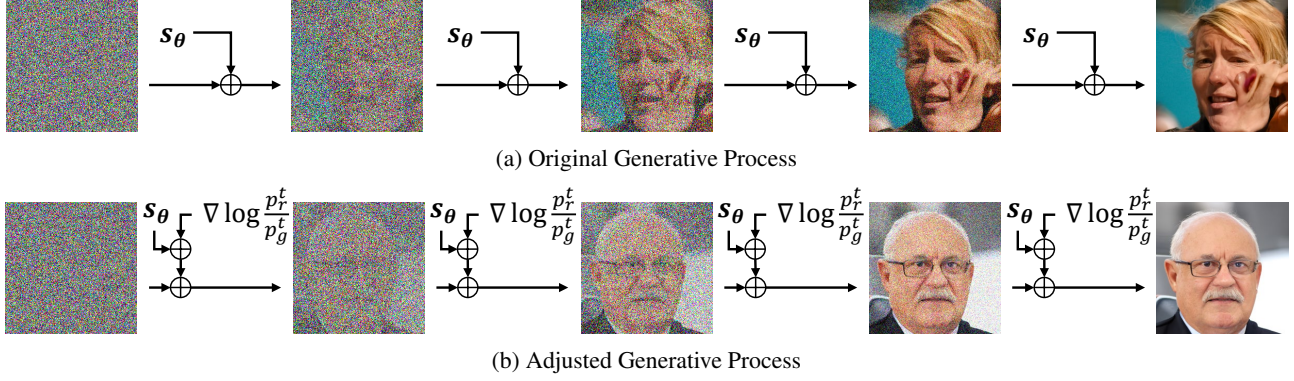


Figure 1: Comparison of the generative processes. (a) The generative process does not directly maximize the density ratio $\frac{p_r^t}{p_g^t}$. (b) The adjusted generative process guides the sample to maximize the density ratio $\frac{p_r^t}{p_g^t}$. The density ratio is modeled by a time-embedded discriminator by $\frac{p_r^t}{p_g^t} \approx \frac{d_\phi}{1-d_\phi}$.

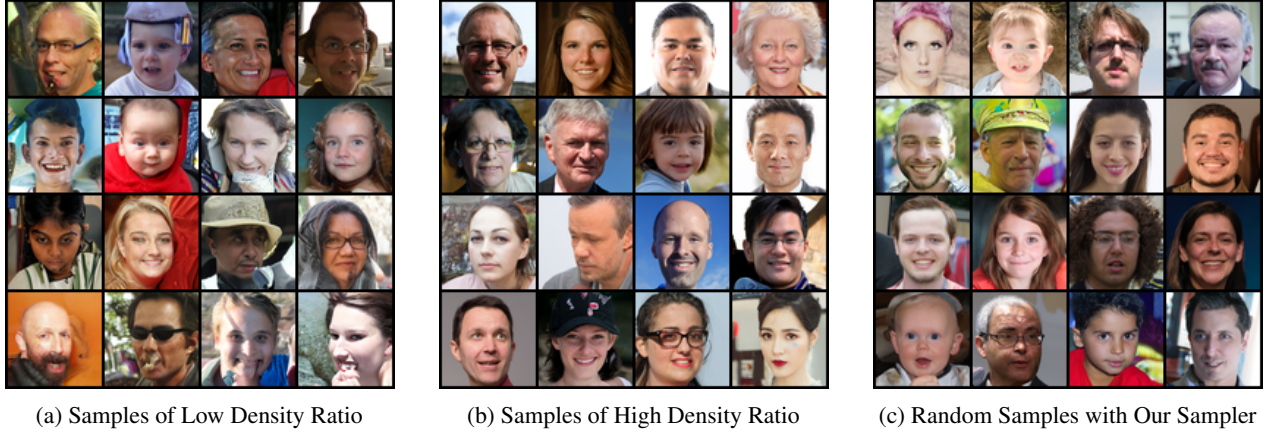


Figure 2: Comparison of generated samples on FFHQ. (a) The bottom 16 samples sorted by the density ratio out of 100 generated samples. (b) The top 16 samples by the density ratio in the same batch of 100 samples. (c) Random samples from the proposed generative process with discriminator guidance.

the suggested technique is applicable both in discrete and continuous settings.

There is a unique reverse-time diffusion process

$$d\mathbf{x}_t = \left[-\frac{1}{2}\beta_t\mathbf{x}_t - g_t^2\nabla\log p_r^t(\mathbf{x}_t) \right] d\bar{t} + g_t d\bar{\mathbf{w}}_t \quad (3)$$

that corresponds to the forward process of Eq. (2). Here, \bar{t} and $\bar{\mathbf{w}}_t$ are the time derivative and the Brownian motion with reverse-time, respectively. The diffusion model trains a neural network to estimate the intractable score function with the objective function of

$$\mathcal{L}_\theta = \frac{1}{2} \int_0^T \lambda(t) \mathbb{E}[\|\mathbf{s}_\theta(\mathbf{x}_t, t) - \nabla\log p_r^t(\mathbf{x}_t)\|_2^2] dt. \quad (4)$$

This objective function is the score regression loss, which could be equivalently interpreted as the noise estimation

$$\sum \mathbb{E}[\|\epsilon_\theta - \epsilon\|_2^2] \text{ (Ho et al., 2020) or the data reconstruction } \sum \mathbb{E}[\|\hat{\mathbf{x}}_\theta(\mathbf{x}_t) - \mathbf{x}_0\|_2^2] \text{ (Kingma et al., 2021).}$$

There are various choices for perturbation strategies and network structures. First, we describe the family of perturbation strategies. The Variance Exploding (VE) SDEs (Song et al., 2020) are the types of $d\mathbf{x}_t = g_t d\mathbf{w}_t$ with $\mathbf{x}_t \sim \mathcal{N}(\mathbf{x}_0, \sigma_t^2 \mathbf{I})$, where σ_t is subordinate to g_t . The specific choice of σ_t varies by papers: for instance, Geometric VE (GVE) (Song et al., 2020) has $\sigma_{GVE}^2(t) = \sigma_{min}^2(\frac{\sigma_{max}}{\sigma_{min}})^{2t}$, and Weighted VE (WVE) (Karras et al., 2022) defines $\sigma_{WVE}^2(t) = (\sigma_{min}^{\frac{1}{\rho}} + t(\sigma_{max}^{\frac{1}{\rho}} - \sigma_{min}^{\frac{1}{\rho}}))^{\frac{1}{\rho}}$.

The Variance Preserving (VP) SDEs are defined as Eq. 2. Ho et al. (2020) introduced Linear VP (LVP) with the linear scheduling of $\beta_t = \beta_{min} + t(\beta_{max} - \beta_{min})$, and Nichol & Dhariwal (2021) proposed Cosine VP (CVP) with the cosine scheduling of β_t . Mathematically, all VE/VP SDEs

are equivalent under scale translations. The point, however, is that the equivalent variations perform differently in empirical studies, and it is far-reaching to understand the behavioral differences (Kim et al., 2022a).

For the network structures, we denote DDPM++ and NCSN++ as the structures from Song et al. (2020), ADM and EDM as those from Dhariwal & Nichol (2021) and Karas et al. (2022), respectively. The estimation targets differ by network structures.

3. Refining Generative Process with Discriminator Guidance

3.1. Sampling Error Decomposition

The generative process becomes

$$d\mathbf{x}_t = \left[-\frac{1}{2}\beta_t\mathbf{x}_t - g_t^2\mathbf{s}_\theta(\mathbf{x}_t, t) \right] d\bar{t} + g_t d\bar{\mathbf{w}}_t, \quad (5)$$

and the model distribution p_g becomes the solution of Eq. (5) with a numerical solver. De Bortoli (2022) clarifies that the error between the model and the data originates from three main sources:

$$W_1(p_r, p_g) \leq E_{pri} + E_{est} + E_{sol}, \quad (6)$$

where E_{pri} is the prior mismatch error, E_{est} is the score estimation error, and E_{sol} is the numerical solver error. Previous works on a new sampler mostly focused on refining the numerical solver as to E_{sol} being robust on the discretization step sizes. For an orthogonal direction, this paper deals with the estimation error E_{est} , and we introduce discriminator guidance that could effectively minimize the error.

3.2. Adjusted Generative Process

We propose the adjusted generative process given by

$$d\mathbf{x}_t = \left[-\frac{1}{2}\beta_t\mathbf{x}_t - g_t^2\left(\mathbf{s}_\theta + \nabla \log \frac{p_r^t}{p_g^t}\right) \right] d\bar{t} + g_t d\bar{\mathbf{w}}_t. \quad (7)$$

Eq. (7) adds the gradient of the log density ratio over the original generative process of Eq. (5). This adjusted sampler is essentially equivalent to sampling from p_g and accepts samples of those likelihood ratio p_r^t/p_g^t are high. With this view, the proposed sampler with the adjusted generative process avoids the samples of False Positive (FP), type-I error. Therefore, the adjusted generative process naturally improves the precision by design, where the precision is defined as $\frac{TP}{TP+FP}$ with TP representing True Positive.

Figure 2 illustrates the generated samples from FFHQ. Figure 2-(a,b) shows that the density ratio is a meaningful sample selection criteria because the samples of high density ratio are more realistic than that of low ratio. Figure 2-(c)

Algorithm 1 Sampling with Discriminator Guidance

```

1: Sample  $\mathbf{x}_T \sim \mathcal{N}(0, \sigma_{max}^2 \mathbf{I})$ 
2: for  $i = N$  to 1 do
3:   Sample  $\boldsymbol{\epsilon}_i \sim \mathcal{N}(0, S_{noise}^2 \mathbf{I})$ 
4:    $\hat{t}_i \leftarrow t_i + \gamma_i t_i$ 
5:    $\hat{\mathbf{x}}_i \leftarrow \mathbf{x}_i + \sqrt{\hat{t}_i^2 - t_i^2} \boldsymbol{\epsilon}_i$ 
6:    $\mathbf{d}_{\hat{t}_i} \leftarrow -\frac{1}{2}\beta_{\hat{t}_i}\mathbf{x}_{\hat{t}_i} - \frac{1}{2}g_{\hat{t}_i}^2\mathbf{s}_\theta(\mathbf{x}_{\hat{t}_i}, \hat{t}_i)$ 
7:    $\mathbf{a}_{\hat{t}_i} \leftarrow -\frac{1}{2}g_{\hat{t}_i}^2 \nabla \log \frac{d_\phi(\mathbf{x}_{\hat{t}_i}, \hat{t}_i)}{1 - d_\phi(\mathbf{x}_{\hat{t}_i}, \hat{t}_i)}$ 
8:    $\mathbf{x}_{t_{i-1}} \leftarrow \mathbf{x}_{\hat{t}_i} + (t_{i-1} - \hat{t}_i)(\mathbf{d}_{\hat{t}_i} + \mathbf{a}_{\hat{t}_i})$ 
9: end for
    
```

demonstrates that the samples from the adjusted process are visually equivalent to that of high density ratio.

In fact, the adjusted score guides our generative process to be equal to the reverse process by Theorem 1.

Theorem 1. *The adjusted generative process of Eq. (7) equals the reverse process of Eq. (3) if and only if the evidence lower bound equals the likelihood.*

Moreover, Theorem 2 says more: even though the equality condition of Theorem 1 is not satisfied, Eq. (7) minimizes the score estimation error.

Theorem 2. *Suppose p_{ag} to be the solution of the adjusted generative process of Eq. (7). If*

$$W_1(p_r, p_{ag}) \leq E_{pri} + E'_{est} + E_{sol},$$

then $E'_{est} < E_{est}$.

3.3. Discriminator Guidance

With all the theoretical advantages of the adjusted generative process, however, solving Eq. (7) is infeasible because the log density ratio is intractable. To approximate the ratio $\log \frac{p_r^t}{p_g^t}$, we additionally train a discriminator network $d_\phi(\mathbf{x}_t, t)$ by optimizing the binary cross entropy

$$\begin{aligned} \mathcal{L}_\phi = & \int \lambda(t) (\mathbb{E}_{p_r^t(\mathbf{x}_t)} [-\log d_\phi(\mathbf{x}_t, t)] \\ & + \mathbb{E}_{p_g^t(\mathbf{x}_t)} [-\log (1 - d_\phi(\mathbf{x}_t, t))]) dt, \end{aligned} \quad (8)$$

where λ is the temporal weight. The optimal discriminator of Eq. (8) becomes

$$d^*(\mathbf{x}_t, t) = \frac{p_r^t(\mathbf{x}_t)}{p_r^t(\mathbf{x}_t) + p_g^t(\mathbf{x}_t)}, \quad (9)$$

and the ratio is represented as the optimal discriminator by

$$\nabla \log \frac{p_r^t(\mathbf{x}_t)}{p_g^t(\mathbf{x}_t)} = \nabla \log \frac{d^*(\mathbf{x}_t, t)}{1 - d^*(\mathbf{x}_t, t)}. \quad (10)$$

Table 1: Comparison of our sampler with previous SOTAs.

	CIFAR-10	CelebA	FFHQ
Previous SOTA	2.03	1.90	2.39
+ Discriminator Guidance	1.83	1.34	1.98
+ Rejection ($\alpha \approx 0.8$)	1.75	-	1.89
Rejection ($\alpha \approx 0.4$)	1.74	1.33	1.88

Then, plugging Eq. (10) into the adjusted generative process of Eq. (7) derives the equivalent form of Eq. (7) with

$$d\mathbf{x}_t = \left[-\frac{1}{2}\beta_t\mathbf{x}_t - g_t^2 \left(\mathbf{s}_\theta + \nabla \log \frac{d^*}{1-d^*} \right) \right] d\bar{t} + g_t d\bar{\mathbf{w}}_t.$$

Summing altogether, we define the adjusted generative process with **Discriminator Guidance** by

$$d\mathbf{x}_t = \left[-\frac{1}{2}\beta_t\mathbf{x}_t - g_t^2 \left(\mathbf{s}_\theta + \nabla \log \frac{d_\phi}{1-d_\phi} \right) \right] d\bar{t} + g_t d\bar{\mathbf{w}}_t. \quad (11)$$

Algorithm 1 describes the full details of our sampling procedure. Without line 7, the sampler is equivalent to that of Karras et al. (2022). In Algorithm 1, S_{noise} and γ_i are chosen according to Karras et al. (2022).

4. Experiments

We experiment on CIFAR-10, CelebA 64x64, and FFHQ 64x64 with unconditional generation. We compare our sampler (Algorithm 1) with the unadjusted vanilla sampler of Karras et al. (2022) (Algorithm 1 without line 7). We use the pre-trained checkpoints from Karras et al. (2022) for CIFAR-10 and FFHQ. For CIFAR-10, we compare the samples from the original and adjusted generative processes with 35 NFEs for sample generation. In this dataset, the released code generates samples with an FID of 2.03, a bit worse than the reported value (1.97) from Karras et al. (2022). We sample FFHQ with 71 NFE, and CIFAR-10 with 35 NFE. Otherwise, we fix all hyperparameter configurations to the baseline sampler. For CelebA, we use the checkpoint from Kim et al. (2022b) and compare samples from the probability flow ODE.

Quantitative Analysis Table 1 presents that our sampler beats the previous sampler on all datasets. Also, we conclude that our sampler performs close to the rejection sampler without significantly increasing NFE per sample. Motivated by Figure 2, the rejection sampler rejects samples of low quality. It rejects generated samples with discriminator values less than 0.5 and accepts samples with values greater than 0.5. The value of 0.5 is equivalent to the density ratio of 1 by

$$d_\phi(\mathbf{x}, 0) \geq 0.5 \iff \frac{p_r(\mathbf{x})}{p_g(\mathbf{x})} \approx \frac{d_\phi(\mathbf{x}, 0)}{1 - d_\phi(\mathbf{x}, 0)} \geq 1.$$

Therefore, the rejection sampler filters out the samples with density ratios less than 1, which means that all the unrealistic samples are rejected.

The discriminator guidance improves the sample quality further by combining it with the rejection criteria. The acceptance probability α of the original unadjusted sampler is approximately 40% in Table 1. Therefore, only 2 out of 5 samples are accepted with the original sampler, requiring approximately 2.5x NFE per sample with the rejection scheme. On the other hand, our sampler guides the sample path on the region of the high density ratio. Consequently, about 4 out of 5 samples are accepted with the discriminator guidance, and it needs only 1.25x NFE per sample to make it comparable with the original rejection algorithm.

Qualitative Analysis Figure 3 compares two of the generative processes with the data forward process on FFHQ. Figure 3-(a) illustrates that the generative process adjusted with the discriminator guidance aligns with the data forward (=reverse) process, whereas the original generative process misfits to the data forward process. Figure 3-(b) shows the histogram and the density plot of the log density ratio with no perturbation of $\sigma(t) = 0 \iff t = 0$. Analogous to Figure 3-(a), the generative process with discriminator guidance generates samples of data-like log density ratio in Figure 3-(b).

Ablation Study Figure 4 studies the effect of discriminator guidance by NFE. It implies that the discriminator guidance is widely effective in all NFEs but the smallest NFE of 19 on CIFAR-10, and we leave it as a future work. It is worth noting that the sweet spot of the optimal NFE of the adjusted process is reduced for both CIFAR-10 and FFHQ compared to the original process.

5. Conclusion

This paper improves the generative process of diffusion models with the discriminator. The auxiliary information of discriminating power guides samples on the region of high density ratio, $\frac{p_r}{p_g}$. This guidance is effective in improving the sample quality, and we achieve the new SOTAs on every dataset we tested on.

References

- De Bortoli, V. Convergence of denoising diffusion models under the manifold hypothesis. *arXiv preprint arXiv:2208.05314*, 2022.
- Dhariwal, P. and Nichol, A. Diffusion models beat gans on image synthesis. *Advances in Neural Information Processing Systems*, 34, 2021.
- Goodfellow, I., Pouget-Abadie, J., Mirza, M., Xu, B., Warde-

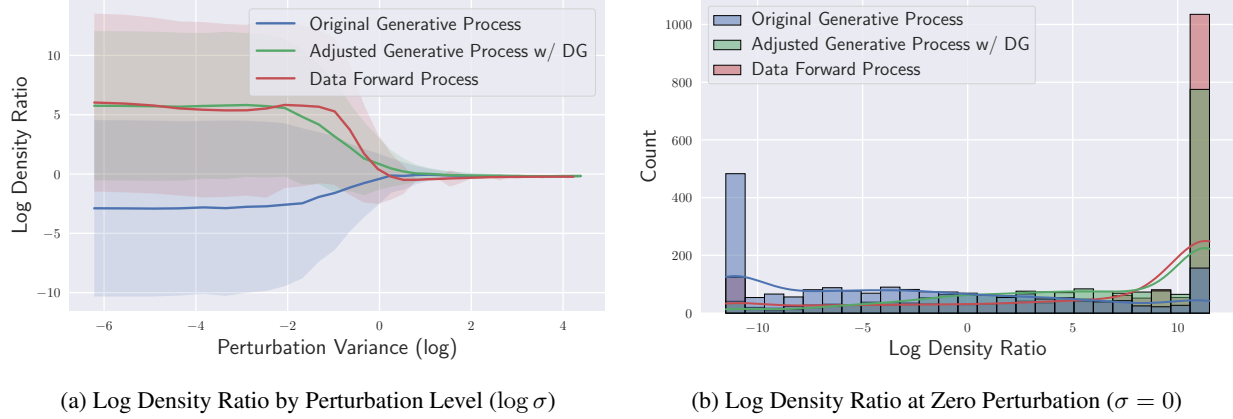


Figure 3: Comparison of the generative processes and the data forward process on FFHQ with respect to the log density ratio. When training, we truncate the discriminator value from 10^{-5} to $1 - 10^{-5}$ to avoid numerical instability, which explains the bound of the log density ratio to be $-11 \lesssim \log \frac{p_r}{p_g} \approx \log \frac{d_\phi}{1-d_\phi} \lesssim 11$.

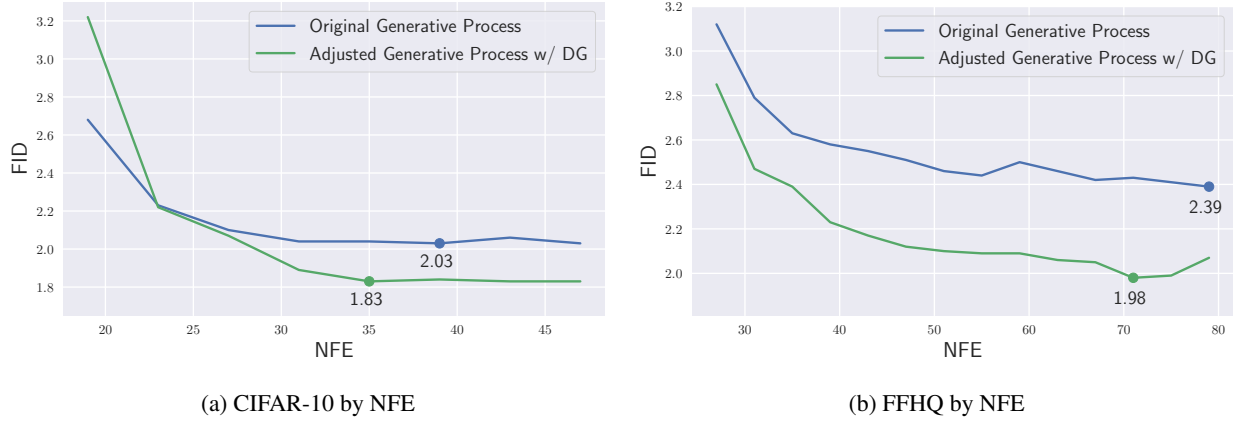


Figure 4: Comparison of the generative processes with respect to NFE on CIFAR-10 and FFHQ.

Farley, D., Ozair, S., Courville, A., and Bengio, Y. Generative adversarial networks. *Communications of the ACM*, 63(11):139–144, 2020.

Ho, J., Jain, A., and Abbeel, P. Denoising diffusion probabilistic models. *Advances in Neural Information Processing Systems*, 33:6840–6851, 2020.

Ho, J., Saharia, C., Chan, W., Fleet, D. J., Norouzi, M., and Salimans, T. Cascaded diffusion models for high fidelity image generation. *arXiv preprint arXiv:2106.15282*, 2021.

Ho, J., Salimans, T., Gritsenko, A., Chan, W., Norouzi, M., and Fleet, D. J. Video diffusion models. *arXiv preprint arXiv:2204.03458*, 2022.

Karras, T., Laine, S., and Aila, T. A style-based generator architecture for generative adversarial networks. In

Proceedings of the IEEE/CVF Conference on Computer Vision and Pattern Recognition, pp. 4401–4410, 2019.

Karras, T., Aittala, M., Aila, T., and Laine, S. Elucidating the design space of diffusion-based generative models. *arXiv preprint arXiv:2206.00364*, 2022.

Kim, D., Na, B., Kwon, S. J., Lee, D., Kang, W., and Moon, I.-C. Maximum likelihood training of implicit nonlinear diffusion models. *arXiv preprint arXiv:2205.13699*, 2022a.

Kim, D., Shin, S., Song, K., Kang, W., and Moon, I.-C. Soft truncation: A universal training technique of score-based diffusion model for high precision score estimation. In *International Conference on Machine Learning*, pp. 11201–11228. PMLR, 2022b.

Kingma, D. P. and Welling, M. Auto-encoding variational bayes. *arXiv preprint arXiv:1312.6114*, 2013.

- Kingma, D. P., Salimans, T., Poole, B., and Ho, J. Variational diffusion models. In *Advances in Neural Information Processing Systems*, 2021.
- Krizhevsky, A., Hinton, G., et al. Learning multiple layers of features from tiny images. 2009.
- Liu, Z., Luo, P., Wang, X., and Tang, X. Deep learning face attributes in the wild. In *Proceedings of the IEEE international conference on computer vision*, pp. 3730–3738, 2015.
- Nichol, A. and Dhariwal, P. Improved denoising diffusion probabilistic models. *arXiv preprint arXiv:2102.09672*, 2021.
- Ramesh, A., Dhariwal, P., Nichol, A., Chu, C., and Chen, M. Hierarchical text-conditional image generation with clip latents. *arXiv preprint arXiv:2204.06125*, 2022.
- Rombach, R., Blattmann, A., Lorenz, D., Esser, P., and Ommer, B. High-resolution image synthesis with latent diffusion models. In *Proceedings of the IEEE/CVF Conference on Computer Vision and Pattern Recognition*, pp. 10684–10695, 2022.
- Saharia, C., Chan, W., Saxena, S., Li, L., Whang, J., Denton, E., Ghasemipour, S. K. S., Ayan, B. K., Mahdavi, S. S., Lopes, R. G., et al. Photorealistic text-to-image diffusion models with deep language understanding. *arXiv preprint arXiv:2205.11487*, 2022.
- Singer, U., Polyak, A., Hayes, T., Yin, X., An, J., Zhang, S., Hu, Q., Yang, H., Ashual, O., Gafni, O., et al. Make-a-video: Text-to-video generation without text-video data. *arXiv preprint arXiv:2209.14792*, 2022.
- Song, Y., Sohl-Dickstein, J., Kingma, D. P., Kumar, A., Ermon, S., and Poole, B. Score-based generative modeling through stochastic differential equations. In *International Conference on Learning Representations*, 2020.
- Voleti, V., Jolicœur-Martineau, A., and Pal, C. Mcvd: Masked conditional video diffusion for prediction, generation, and interpolation. *arXiv preprint arXiv:2205.09853*, 5(4.1):4, 2022.